Modeling of a Pulsed Plasma Thruster; Simple Design, Complex Matter

Peter Shaw and Vaios Lappas
Surrey Space Center, University of Surrey, Guildford, GU2 7XH, UK
p.shaw@surrey.ac.uk

April 26, 2010

Abstract

Experiments conducted at the Surrey Space Centre on a breadboard pulsed plasma thruster (PPT) have led to greater insights in to the underlying principles of electrode erosion during plasma formation. It has been shown that during a PPT discharge a significant proportion of the plasma that is produced is from direct erosion of the electrodes to the extent that traditional Teflon propellant bars were removed from the PPT and it remained operational. The removal of the propellant bar allowed a direct relationship between the plasma mass and the eroded mass to be constructed. Research from the metal film deposition and cathodic plasma fields was then drawn upon to create a model for the eroded mass. This model was then expanded and used to predict the current profile of a discharging PPT and compared to experimental current profiles using a rogowski coil.

Introduction

The pulsed plasma thruster has a long established history with the first flight being on the Zond-2 satellite in 1964. Despite the fact that it is simple to build and operate it is still considered, even after 50 years, one of the most complex devices to understand from the point of view of its under pinning physical principles, which has led to a multitude of inefficient PPT designs (typically below 20%). Despite this PPTs are a main contender for an electric propulsion solution for small satellites because of their low power consumption, reliability, low mass and reasonable specific impulse. Recent years have seen a number of flight demonstrated or flight qualified hardware including the EO-1 PPT experiment [1], Dawgstar PPT module [2], SIMP-LEX [3], and JOSHO [4]. The PPT is an Electric Propulsion (EP) device that uses the electromagnetic force to accelerate a plasma sheet in an accelerator chamber consisting of metal electrodes in some form of configuration. The energy used to produce and accelerate the plasma comes from a high voltage (HV) capacitor connected in parallel with the electrode configuration, the HV capacitor is charged becoming an energy bank. PPT's discharge at a variety of energy levels dependent on circuit parameters with discharge energies ranging from J to kJ [5]. Electrode configurations have come in many forms from the standard coaxial and parallel plate versions to the exotic side feed, flared and tongued configurations [2, 6, 7]. A discharge initiator (DI) is used to initiate the discharge, this can be a sparkplug, a semiconductor sparkplug [6], undervoltage breakdown through electron pulse injection [8], surface breakdown [9] or a mechanical trigger [10]. During experimentation it was found that a negatively biased 15kV tungsten filament located 10mm from the cathode surface could also induce a thermo-field emission and initiate the discharge. The exact nature or process of how the DI initiates the PPT discharge is not well understood and studies have been limited [11, 12]. It can be shown that the method of initiation has an overall effect on the discharge of the PPT, see Figure 1.

Once initiation by the DI has begun a plasma bulk forms in between the electrodes, this bulk plasma is subjected to the Lorentz force ($j \times B$) that is created by the current passing through the plasma skin of the plasma bulk from one electrode to the other and the strong magnetic fields that are setup as current flows through them. The energy for the formation of the bulk plasma comes from a high voltage capacitor that is attached in parallel to the electrodes, so as the discharge propagates a characteristic LCR signal is produced, see Figure 1 and 2. Experiments done with high speed cameras at Universität Stuttgart show during the initial ringing period, when the voltage reverses across the capacitor terminals a new plasma sheet is created until the environment within the discharge area becomes stable enough for plasma sheaths to form and then a thermal plasma is produced, see Figure 3 [13].

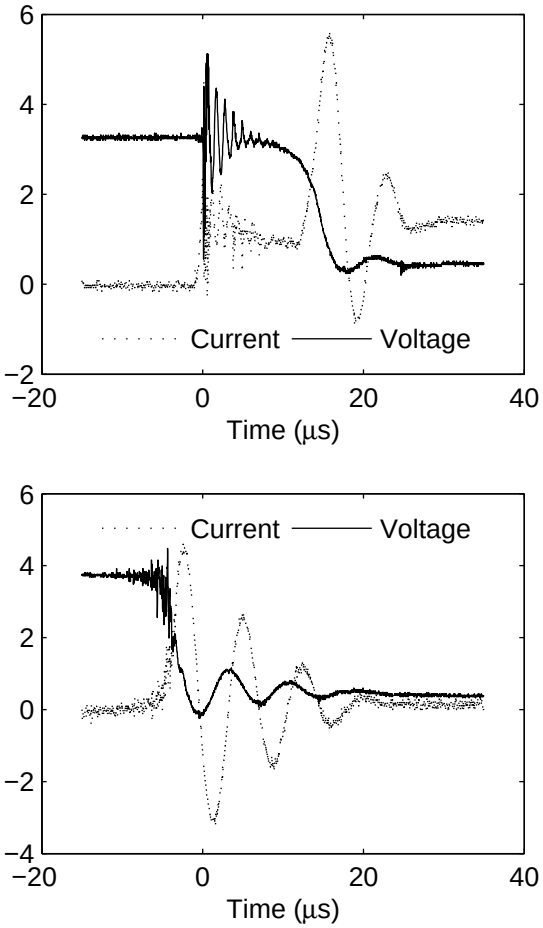

Figure 1: Current and voltage profiles showing two types of discharge (from two different discharge initiators), Top: Thermionic emission (sparkplug 'glow' discharge), Bottom: Thermo field emission (negatively biased 15kV tungsten filament). The voltage is measured across the capacitor and the current measured by Rogowski coil around the anode. On the Y-axis, current is 500A per unit and voltage is 500V per unit

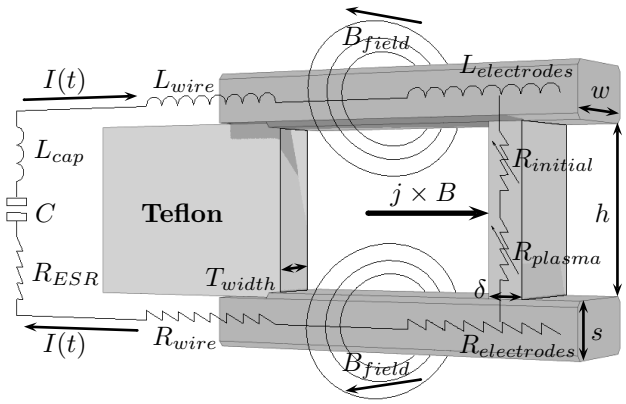

Figure 2: A circuit schematic overlaid on the main components of a PPT, depicting the origin of the Lorentz force that accelerates the plasma sheet

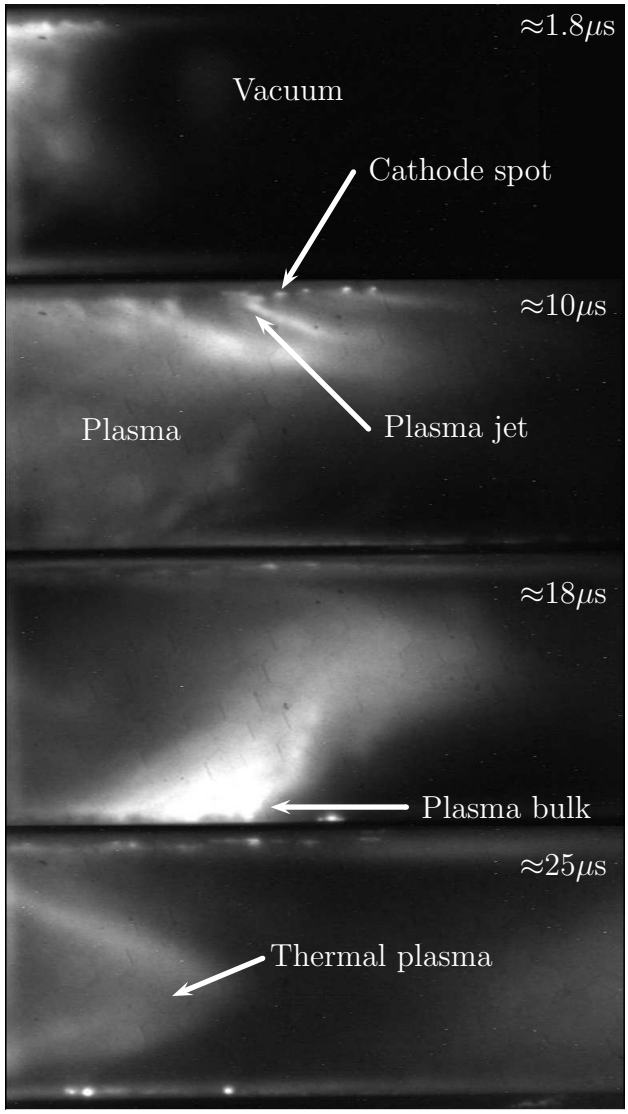

Figure 3: From top to bottom respectively; 1) Initial breakdown of plasma, 2) First discharge with substantial bending of plasma jets due to high magnetic fields and large kA currents, 3) Second discharge forming on the bottom electrode due to polarity reversal of the capacitor with large numbers of plasma jets forming a significant bulk plasma, 4) Thermal plasma production. Bright spots in the picture are cathode spots which are accompanied by plasma jet production, exposure time for each frame is 20ns [13]

The acceleration of the plasma bulk and the processes that occur after the discharge of the plasma bulk are better understood, for instance once the plasma bulk is ejected additional processes occur which release neutral vapours, create macro-particles and deposit carbon within the PPT, these all cause poor performance and in the long term failure within PPTs. An area that remains underdeveloped is the understanding of the formation of the plasma during the PPT discharge. Traditional thinking is that the majority

of the mass that creates the plasma bulk originates from the Teflon surface, our studies show that this is only the case for certain low energy regimes and in most cases the majority of the mass actually comes from the erosion of the electrodes, see Figure 4.

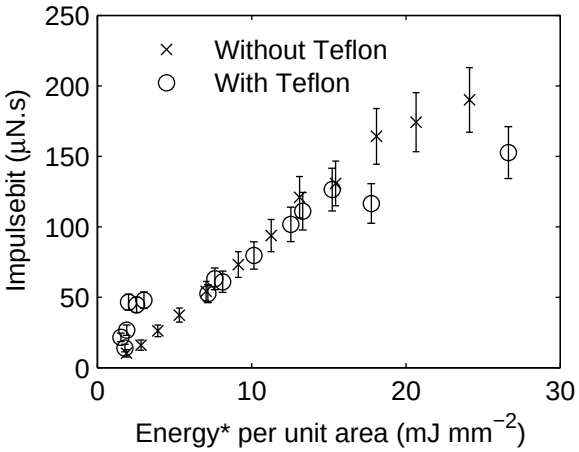

Figure 4: Impulse bit compared with energy per unit area of a PPT discharge with and without Teflon

It is believed that mass erosion of the electrodes occurs in a similar fashion seen in the cathodic arc and metal deposition fields, where ion bombardment of areas of negatively charged areas (promoted by steep field gradients of uneven surfaces) create areas of thermal runaway which lead to a 'micro explosion' and formation of craters, see Figure 5 and 6.

During a cathodic discharge dependent on the passing current there is a number of 'micro explosions' otherwise known as cathode spots and due to there close proximity to each other the individual plasma jets from each explosion meld into a single plasma flow region of several plasma jets creating the observed plasma bulk, see Figure 7. The plasma bulk is pinched and bent by strong magnetic fields canting the bulk plasma which has often been observed.

Model Development

Modeling in the PPT field has been diverse, with models used to analyse specific situations like the interaction between the Teflon surface and the plasma bulk via a layer model [14] or the expansion and evolution of the plasma plume [15, 16]. 1D and 3D modeling that simulate the overall process have had reasonable degrees of success; MACH is a complete 3D MHD code but is computationally complex [17, 18], the 1 dimensional circuit mass snowplow and mass slug-shot models compile quickly but all tend to be relatively inaccurate in comparison with experimental results [19, 20].

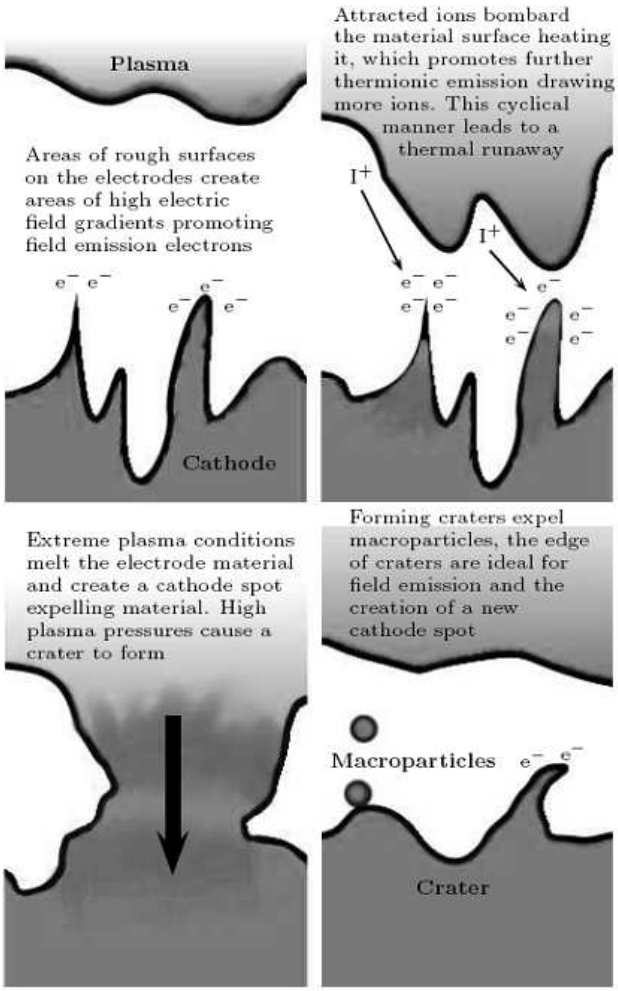

Figure 5: Evolution of the cathode spot process and macroparticle formation as a result of plasma pressure on the super heated cathode material

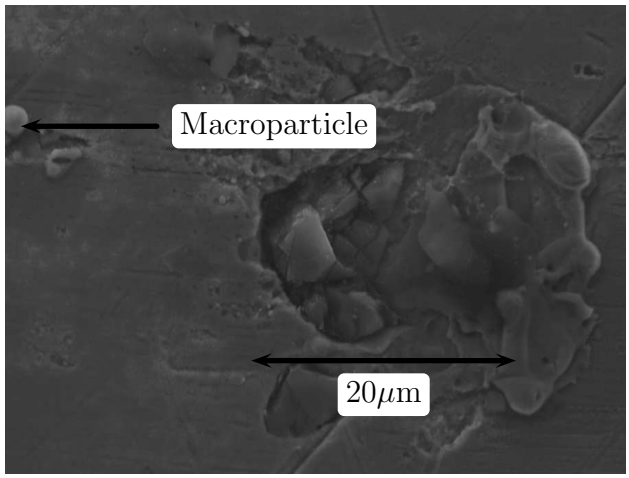

Figure 6: An electron microscope image of a single crater in the copper electrode, in the top left a macroparticle of molten copper can be seen

The model development began with the 1 dimensional circuit mass slug-shot model [19], see

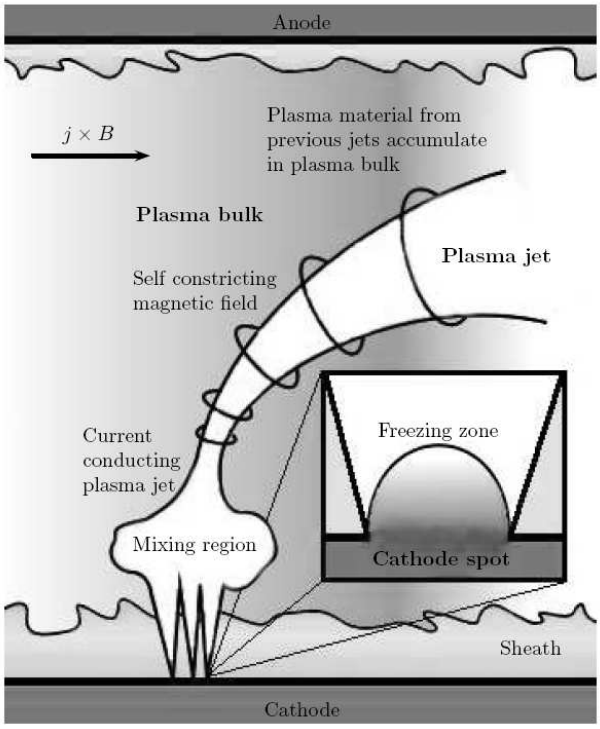

Figure 7: Plasma evolution from emission centre to plasma bulk in a cathode spot plasma jet of a PPT

Equations (1),(2) and (3), but was modified to include time dependent resistive elements that describe the initial breakdown, the cathode spot plasma jet formation and the geometry of the plasma bulk. It directly relates the mass erosion of the electrodes via the emission of cathode spots with the magnitude of current that flows through the electrodes into the plasma. It accounts for the increased electrical resistance in the electrodes due to the skin effect at the frequencies that the PPT discharges at. Finally it treats the overall discharge as a multitude of individual plasma sheets rather than a single plasma formation.

$$\begin{aligned} &V_0 - \frac{1}{C}\int_0^t I(t)dt = ... \\ &...I(t)\left[R_{ESR} + R_{wire} + R_{electrodes} + R_{plasma}\right]... \\ &... + \frac{dI(t)}{dt}\left[L_{cap} + L_{wires} + \mu_0\frac{h}{w}x(t) + \mu_0\frac{h}{w}\frac{\delta}{2}\right]... \\ &... + \frac{dx}{dt}\mu_0\frac{h}{w}I(t) \end{aligned} \tag{1}$$

$$\frac{m(t)}{dt}\frac{dx(t)}{dt} + m(t)\frac{dx^2(t)}{d^2t} = \int_V (j \times B)\, dV \tag{2}$$

$$\int_V (j \times B)\, dV = \frac{1}{2}\mu_0\frac{h}{w}\left[I(t)\right]^2 \widehat{x} \tag{3}$$

Time Dependant Plasma Resistance

Universität Stuttgart, using high speed photography identified three stages of plasma development which are the initial breakdown period, the cathode spot plasma jet production period and the thermal plasma production period, see Figure 3.

Initial Breakdown

The additional resistance in the plasma during the initial breakdown was found by using an empirical fit. This was done by adding a resistive term to the overall plasma resistance that would cause the first peak of the modeled current profile to match with the first peak of the experimental current profile for 3cm electrode separation. This was done for voltages between 700V to 3100V. A relationship was found and was then modified and expanded to account for electrode separations of 1cm and 5cm. For the work done the initial resistance empirical fit was;

$$\begin{aligned} &R_{initial}(t) = \exp(7.6 - 94.22h)... \\ &... \exp(-t \times 10^{-6}\exp(1.25 - 15.72h)) \end{aligned} \tag{4}$$

Where t is the discharge time. The best fit was applied for the first 3μs of the overall discharge process, after which this was set to zero. It is thought that this relationship will differ for different PPT's as other parameters (i.e. capacitance, electrode material) will have an effect. Future work will look at the initial breakdown conditions and processes.

Cathode Spot Plasma Jet

The plasma jet model describes the evolution of the plasma from electrode erosion to plasma bulk. The process starts off with the creation of emission centres. Anders explains the mechanisms of emission centres (cathode spots) in detail [10, 21]. In summary the copper electrodes are not smooth surfaces and on the microscopic scale are 'rough', field emission occurs at geometric sharp points and promotes ion bombardment in these geographic locations, see Figure 5. As ion bombardment increases the area rapidly heats and thermionic emission occurs. The increased presence of electrons promotes further ion bombardment and a thermal runaway occurs which rapidly heats the surface until it 'explodes' and leaves a visible crater, see Figure 6. As this material is expelled it evolves from a dense expanding plasma dominated by collisions into a plasma that has its electrons 'trapped' in the nearby strong magnetic field lines. If this change is rapid than the plasma parameters are 'frozen' and the plasma parameters in the mixing region, which is at a significant distance from the cathode spot, are similar to the conditions that they were at

the freezing zone. The frozen plasma parameters are unique to each element and are summarised by Anders in a periodic table format [10].

If moderate to high current is flowing through the plasma additional affects occur; the number of cathode spots produced at any time increase proportionally to the discharge current, close proximity of these spots create closely packed plasma jets which affect the overall expansion of the plasma jets and can be modeled as a single overall 'plasma flow'. High currents will cause the 'plasma flow' to constrict due to z-pinch dynamics, see Figure 7 [22, 23, 24].

The model developed by Krinberg to explain the internal dynamics of the 'plasma flow' region does not take into account the application of an external magnetic field, created by flowing current in the electrodes that would be present in a PPT. The external field would cause bending of the pinched plasma flow region and bend it in the direction of plasma sheet acceleration, this bending is also refereed to as plasma sheet canting. The effect of canting is not modeled and is left for future work. Anders' work on cathode spots and Krinbergs model on the z-pinch effect of cathode spot plasmas at high current can be consolidated if the mass ion flux $G(t)$ from Krinberg/Krasovs' work [24] is related to the ion erosion rate Γ_i of Anders work [10] by the following expression;

$$G(t) = \frac{I(t)\Gamma_i}{\overline{Q}(t)} \tag{5}$$

With this alteration to Krinbergs model the electron temperature in the plasma jet can be expressed as a function of the flowing current through the plasma jet and the velocity of the plasma jet near the anode surface.

$$T_e(t) = \frac{I(t)\mu_0 m_i v_{jet}(t)}{8\pi k_B \Gamma_i} \tag{6}$$

The plasma flow area of the expanding jet is a function of the radius and jet velocity, which in turn are functions of the distance from the mixing region. The jet velocity v_{jet} is defined as [24];

$$v_{jet}(t) = v_{spot}\left[1 + \frac{I(t)}{I_{spot}} \ln \frac{r_{jet}(t)}{r_{spot}}\right] \tag{7}$$

where I_{spot}, the current across each spot, is found by;

$$I_{spot} = \left(\frac{4\pi m_i v_{spot}}{\xi(t)\mu_0 e}\right) \tag{8}$$

where $\xi(t)$ is the ion particle flux fraction;

$$\xi(t) = \frac{100}{\overline{Q}(t)} \tag{9}$$

The plasma flow region radius $r_{jet}(t)$ can be found by solving;

$$\begin{aligned} &\frac{I(t)}{I_{spot}}\left(\frac{r_{jet}(t)}{r_{spot}} \ln \frac{r_{jet}(t)}{r_{spot}} - \frac{r_{jet}(t)}{r_{spot}} + 1\right) ... \\ &... + \frac{r_{jet}(t)}{r_{spot}} - 1 = \frac{h}{r_{spot}} \tan(45^o) \end{aligned} \tag{10}$$

The plasma sheet thickness δ can be estimated by solving (10) for the middle distance between the electrodes. (7) to (10) can be solved as long as the mean ion charge state is known. The mean ion charge state increases in high discharge currents or the presence of a magnetic field [25, 26, 27, 28]. The mean ion charge state can be approximated by [23];

$$\begin{aligned} \overline{Q}(t) = \sum_{n=1} \Bigg[&Q_n(t) C_n \left(\frac{-r_{spot} - h}{\lambda_{n+1}(t)}\right) ... \\ &... - C_{n-1}\left(\frac{-r_{spot} - h}{\lambda_n(t)}\right)\Bigg] \end{aligned} \tag{11}$$

where C_n is a function of the ion fraction distribution f_n^0 at the freezing point and is expressed as;

$$C_n = \sum_{n=1} f_n^0 \tag{12}$$

and $\lambda_n(t)$ is found by;

$$\lambda_n(t) = \frac{v_{jet}}{k_n(t) n_{e-jet}(t)} \tag{13}$$

where $k_n(t)$ is the ionisation coefficient of the nth charge state level and can be found by;

$$\begin{aligned} k_n(t) = 1 \times 10^{-20} &\left(\frac{8 k_B T_e(t)}{\pi m_e}\right)^{\frac{1}{2}} ... \\ &... \left(\frac{13.6e}{I_{i,n}}\right)^2 \exp\left(\frac{-I_{i,n}}{k_B T_e(t)}\right) \end{aligned} \tag{14}$$

where $I_{i,n}$ is the ionisation energy to take an ion from the n to the $n+1$ charge state. The electron number density in the plasma jet $n_{e-jet}(t)$ can be found by;

$$n_{e-jet}(t) = \frac{I(t)\Gamma_i}{m_i v_{jet}(t) \pi \left[r_{jet}(t)\right]^2} \tag{15}$$

The total electron number density $n_{e-total}(t)$ in the plasma bulk can be found by;

$$n_{e-total}(t) = \int_0^t \frac{\Delta n_{e-total}(t)}{\Delta \tau} dt \tag{16}$$

where τ is a suitably small change in time compared to the overall discharge, in the model developed an arbitrary value of 0.1μs was used.

Plasma is 'insulated' from the environment that surrounds it by the natural sheaths that are created whenever plasma interacts with a surface. The sheath is a dynamic entity with a structure and thickness that depends on the potential difference between the solid surface and the plasma potential. Stable sheaths are established on timescales of several tens of microseconds which are equivalent to the discharge time of a PPT. So the environment is changing from a no sheath region to a non stable sheath region to a stable sheath region, which could explain the different plasma formations seen in Figure 3, at 10μs sheaths have not yet been established whilst later on at 25μs they have. The evolution of the sheath makes the problem significantly complex which is beyond the scope of this work, however assumptions are made to simplify the situation. From the plasma jet characteristics the plasma potential of a current carrying plasma can be estimated using [29];

$$V_{plasma}(t) = \frac{k_B T_e(t)}{e} \ln\left(\frac{I(t)}{I_{thermal}(t)}\right) \quad (17)$$

where $I_{thermal}(t)$ is the electron current from the plasma bulk to the anode determined by thermal random motion;

$$I_{thermal}(t) = -\frac{1}{4} e n_{e-total}(t) \left(\frac{8 k_B T_e(t)}{\pi m_e}\right) \quad (18)$$

The ion current between the region of the plasma jet and anode electrode is limited and is described by Childs' law [30, 31], but because a stable sheath has not yet formed we assume the distance between the electrodes (as used in vacuum diode analysis) is an adequate choice;

$$I_i(t) = \frac{4}{9}\epsilon_0 \left(\frac{2e}{m_i}\right)^{\frac{1}{2}} \frac{|V_{absolute}(t)|^{\frac{3}{2}}}{h^2} \quad (19)$$

where $V_{absolute}$ is the absolute potential difference between the biased electrode (equivalent to the potential difference seen across the HV capacitor) and the plasma jet potential. For each metal there is a normalisation ratio α_i between ion current $I_i(t)$ and the arc current $I_{arc}(t)$ [10];

$$\alpha_i = \frac{I_i(t)}{I_{arc}(t)} \Rightarrow I_{arc}(t) = \frac{I_i(t)}{\alpha_i} \quad (20)$$

Knowing the arc current between the plasma jet and the anode allows for the estimation of an equivalent plasma resistance $R_{plasma}(t)$ using Ohm's law;

$$R_{plasma}(t) = \frac{V_{absolute}(t)}{I_{arc}(t)} + R_{initial}(t) \quad (21)$$

Thermal Plasma Production

The origin of the thermal plasma is not well defined and could be from the evaporation of material from the Teflon surface or from the natural occurrence of current flowing through plasma once stable sheaths are established. The thermal plasma was not modeled due to it being a process happening in the latter stages of the discharge when discharge currents are relatively low and so it has a relatively small impact on the current profile.

Relating Mass Erosion to Current Flow

Electrode mass erosion occurs by the creation of electron emission sites that interact with local plasma causing thermal runaway in the local surface temperature and causing a micro explosion [10]. Electron emission sites and cathode spot creation is beyond the scope of this paper but a relationship between the ion erosion rate and the arc current has been established. The ion erosion rate is assumed to be equivalent to the mass ablation rate of the electrodes. The total mass ablation of the electrodes if experimentally measured would be higher due to macro particle ejection and the ejection of neutral particles. Macro particles would be accelerated at a much slower speed than plasma ions and electrons due to their increased mass which would lead to discrepancies between thrust measurements. In the scope of this model macro particles are ignored as this is a process that occurs at a time much later than the electromagnetic acceleration of the plasma sheet and so does not affect the discharge profile of the current and voltage signals. The neutral particles (metal atoms) need closer consideration, they interact with plasma and cause a charge exchange collision to occur that could be accelerated electromagnetically, e.g.

$$\mathrm{Cu}^{++} + \mathrm{Cu}^{Neutral} = \mathrm{Cu}^{+} + \mathrm{Cu}^{+} \quad (22)$$

Within the violent process of the micro explosion on the copper electrode large number densities and energies are obtained leading to high ionisation rates [21]. Arc experiments with high temporal resolution have measured the mean ion charge state of copper to be 3.53 3μs after discharge initiation and 2.03 150μs after discharge initiation for currents of around 300A [32]. At peak currents of around 4kA the mean ion charge was $\approx$6 for various cathode materials [28]. The average pulse discharge time of a PPT is in the order of 20μs and maximum peak currents are in the kA range, with these discharge currents and on this timescale the plasma is highly ionised. After the initial micro explosion the plasma expands from plasma dominated by particle collisions to

plasma dominated by particle gyration around the strong magnetic field lines as the plasma density decreases. Recombination by particle collision is significantly reduced and so is not considered to affect the model in the highly ionised plasma sheet. Neutrals from cooling emission sites may also occur but these happen at a later stage and do not effect the acceleration of the plasma sheet. A relationship between mass and discharge current can be obtained;

$$\frac{dm(t)}{dt} = \frac{dm}{dQ}\frac{dQ}{dt} \Rightarrow \Gamma_i I(t) \tag{23}$$

The mass at any given time;

$$m(t) = \Gamma_i \int_0^t I(t)dt \tag{24}$$

From (2), (3), (23) and (24) we complete the mass model;

$$\Gamma_i I(t)\frac{dx(t)}{dt} + \frac{dx^2(t)}{d^2t}\Gamma_i \int_0^t I(t)dt = ... \\ ...\frac{1}{2}\mu_0 \frac{h}{w}\left[I(t)\right]^2 \tag{25}$$

Multiple Plasma Sheet Formation

A current ringing effect can be observed across the terminals of the HV capacitor in a PPT discharge, the discharge begins with the capacitor being held at a specified potential. The discharge is initiated by a DI circuit which effectively closes the circuit between the electrodes, the capacitor begins to discharge but the current is limited by the total circuit resistance and inductance. The discharge operates as an LCR circuit. A plasma sheet forms and under the effects of the Lorentz force it is accelerated down the discharge channel. As current tends to zero the rate of change in voltage also tends to zero. At this stage the voltage will be at a maximum value of opposite polarity compared to when it first began. Spanjers showed that electron densities were at there highest when discharge voltage was also at a maximum causing re-ignition [33]. A second discharge initiates creating another plasma sheet which is then accelerated, the process will continue in this cyclical fashion until the environment and electrical characteristics between the electrodes is such that a plasma sheet cannot form.

The developed model is based on treating each pulse of the current discharge as a separate formation of the plasma sheet. Initial boundary conditions are set by the previous pulse but certain conditions are reset i.e. initial mass, plasma sheet speed and the distance the plasma sheet has traveled. This creates a discontinuous stepped profile to the mass model, see Figure 8

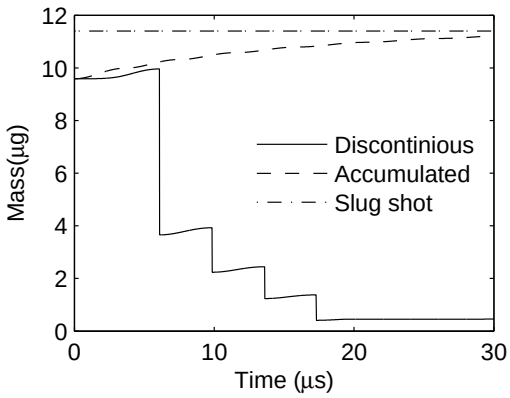

Figure 8: Comparison of mass models for a PPT discharge

The slug shot mass model assumes that the mass of the plasma sheet is constant throughout the discharge. The accumulative mass model (i.e. snowplow model) assumes all the mass is scooped up in one plasma sheet and is accelerated. The discontinuous method accelerates the plasma mass in multiple plasma sheets each one having less mass than the previous. The initial mass m_0 in each step of the discontinuous mass model was calculated by;

$$m_0 = \widetilde{\Gamma}_i E_{discharge}(t) \tag{26}$$

where $E_{discharge}(t)$ is the energy of the capacitor at the start of the subsequent pulse given by;

$$E_{discharge}(t) = \frac{1}{2}C\left[V(t)\right]^2 \tag{27}$$

where the voltage is the discharge voltage at the point, where no current flows between the electrodes (i.e. $I = 0$).

Capacitor Resistance

The resistance of the high voltage capacitor is non ideal, at high frequencies the Equivalent Series Resistance (ESR) of the capacitor decreases. Figure 9 shows a log plot of the ESR as a function of driving frequency using a high frequency (kHz)- low voltage ESR meter. If a best fit is applied to the plot and extrapolated an estimation of 20mΩ for the ESR can be made at a frequency of 130kHz which is equivalent to that of the discharge frequency of the PPT. This estimation should be accepted cautiously as the capacitor could change its non-linear behaviour in the high frequency (kHz) - high voltage regime and further work is required in diagnosing this ESR.

Electrode Skin Effect

At high frequencies the current density distributes itself so it is greater at the surface of the metal electrodes than at the core, the skin

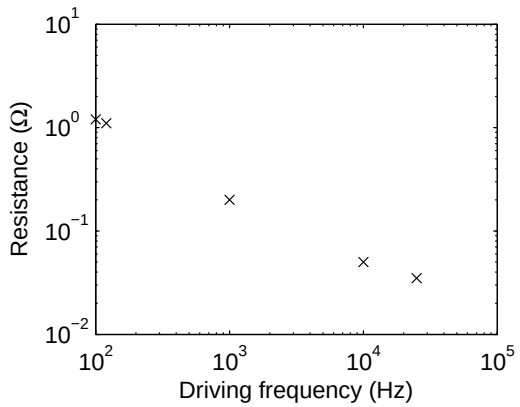

Figure 9: ESR measured across the HV capacitor as the ESR probe driving frequency is varied

effect causes the effective resistance of the electrodes to increase as the discharge frequency increases. The resistance of the electrode can be found from the electrical resistivity and assuming a hollow electrode with wall thickness that equals the depth of the skin effect;

$$R_{electrode} = \frac{\rho_{electrode}}{2\delta_{skin}} \left[\frac{l}{w + s - 2\delta_{skin}} \right] \quad (28)$$

The skin depth can be calculated by;

$$\delta_{skin} = \frac{1}{\sqrt{\pi \mu_0}} \sqrt{\frac{\rho_{electrode}}{\mu_r f}} \quad (29)$$

Boundary Conditions

The model implementation used the Matlab dde23 delayed differential equation solver. The toolset of this solver allowed 'events' to be set that if obtained would terminate the solver. Parameters could then be altered and the solver would then be restarted using the terminated solution and altered parameters to become the new boundary conditions and 'history' for the next pulse. The methodology follows Laperriere's work [34] by solving in state space whilst the plasma jet model is used to calculate the time variant plasma resistance which is implemented at every time step. The initial conditions are summarised in Table 1.

Model Results

To determine the accuracy of the model, the modeled current profile was compared to measured data without Teflon. Figure 10 shows the compared profiles at electrode separations of 1cm, 3cm and 5cm with comparable discharge energies of 7.2J, 6.8J and 6.3J respectively. In general the modeled current profiles are good fits to experimental data, however a few discrepancies can be seen. At 1cm electrode separation there is a definitive current spike at 4μs from 5kA to 8kA and a current spike at 7μs from -4kA to 5kA. These two spikes do not appear at larger electrode separations, which indicate a currently non identified process that occurs on smaller scales that will need to be investigated.

Additionally at 3cm and 5cm the current signal abruptly ends at 22.5μs and 14μs respectively due to significant increases in plasma resistances within the model. The general trend at similar discharge energies is that as electrode separation is increased the peak current signals and signal ringing period decreases. This means that for the same amount of energy being discharged, at larger separations, more energy is being supplied to fewer plasma sheets, showing improved power coupling from the capacitor to the plasma, allowing for more energy per plasma sheet to be converted into kinetic energy to accelerate each individual plasma sheet leading to a more efficient process.

Table 1: Initial conditions; plasma jet initial conditions are taken for copper as published by Anders[10] and Krasov[24]

Initial condition	**Value**
High Voltage Capacitor	
Capacitor type	Polypropylene & oil
Capacitance	4.06μF
Capacitor resistance	≈20mΩ
Discharge Initiator (DI)	
Charging voltage	30kV
DI Capacitance	10nF
Electrodes	
Material	Copper
Width	20mm
Thickness	10mm
Discharge channel length	60mm
Total length of material	520 - 560mm
Connector resistance	≈5mΩ
Skin effect resistance	≈0.9mΩ
Plasma Jet[10]	
Mean ion charge state	2.06
Electron-ion flux ratio	110%
α_i	11.4
Γ_i	33.4μgC^{-1}
$\widetilde{\Gamma}_i$	1.420μgJ^{-1}
Freezing zone/mixing region	
- Spot velocity	13.2kms^{-1}
- Expanding angle	45^o
- Region diameter	0.5mm
- Ion fraction dist.	1+ =10.7%
	2+ =72.1%
	3+ =17.1%
	4+ =0.014%

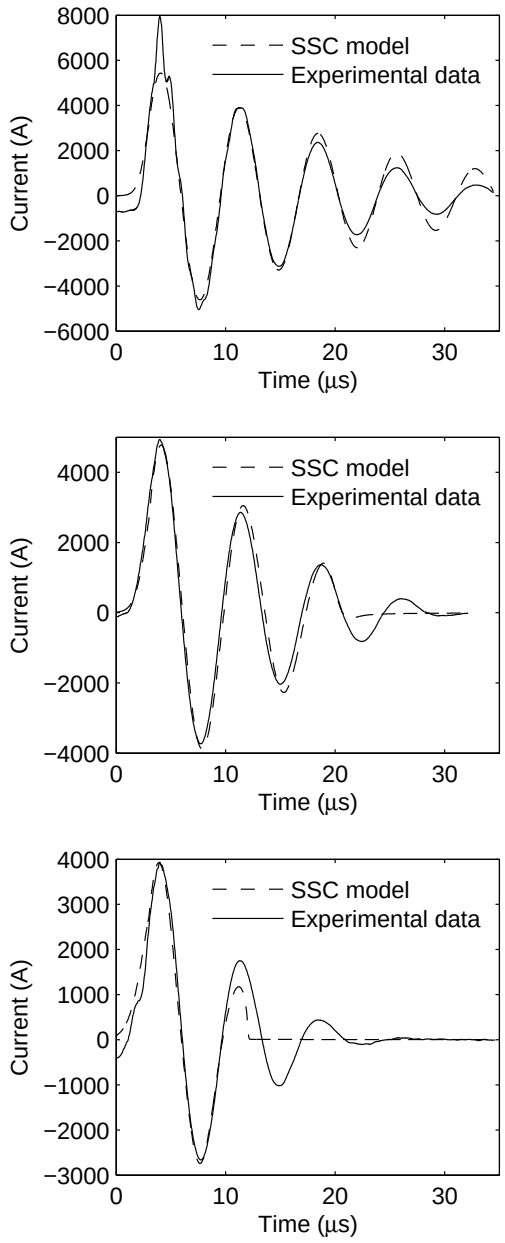

Figure 10: Comparison between averaged experimental data and modeled current profiles of similar discharge energies at a variety of electrode separations Top; 7.2J at 1cm. Middle; 6.7J at 3cm. Bottom; 6.3J at 5cm

Plasma Sheet Dynamics

The model allows for an insight into the dynamics of the plasma sheet, Figure 11 shows the evolution of the energy processes of the PPT discharge, the mean ion charge state of the plasma, the bulk electron number density, the plasma temperature and the total circuit resistance. The bulk plasma temperature is assumed to be equivalent to the plasma jet temperature measured near the surface of the anode.

Figure 11 shows the modeled energy discharge characteristics of a 6.8J discharge at 3cm electrode separation. The stored energy in the capacitor is released and discharged into the plasma over a period of 4.3μs; the energy is converted into kinetic energy ($\approx$ 0.03J) that accelerates the plasma sheet, energy that is lost by particle collisions by joule (ohmic) heating ($\approx$ 2.75J) and energy that is stored within the plasma magnetic field ($\approx$ 3.85J). Joule heating is a measure of the energy lost due to collision affects within the plasma, as joule heating increases so does the electron temperature ($\approx 10^6 K$), particles become more energetic and collision rates increase. This electron temperature is comparable to results in Krinbergs work[23]. The energy is used to ionise the plasma increasing the mean ion charge state ($\approx$ 7.5). As the particles become ionised additional electrons are introduced into the plasma increasing the electron number density ($\approx 10^{19}\mathrm{m}^{-3}$). The circuit resistance decreases as the electron mobility rises. The increased electron mobility allows for high currents to flow through the plasma (Figure 10 $\approx$ 5kA) which induces strong magnetic fields that store energy within them. Once the capacitive energy has been depleted (at 4.3μs) the electron temperature and bulk electron density begin to decrease, the mean ion charge begins to fall, meaning electron and heavy particle recombination occurs. Current mobility decreases and the plasma resistance increases. The energy stored in the magnetic field is released as electron mobility decreases releasing the energy into the plasma which is predominantly used to recharge the plates of the capacitor but further losses do occur due to joule heating. Only a small proportion is usefully converted into kinetic energy to accelerate the plasma sheet. At the end of the discharge (at 6.1μs) the model assumes the plasma sheet has been accelerated out of the thruster and the whole process restarts and repeats itself.

During the initial discharge the energy used in joule heating is significantly higher than in subsequent discharges where joule heating losses remain relatively constant between 1.1J to 0.5J per plasma sheet, the joule heating losses in each sheet diminish the capacitive stored energy until the capacitor is drained. Peak bulk plasma electron densities and temperatures of each discharge gradually decrease and so plasma resistance gradually increases. Peaks within the resistance profile occur when the plasma sheet has been expelled from the discharge chamber, so plasma current is minimal and a new plasma sheet is about to initiate. The electron number density profile is similar to the work presented by Zwahlen who studied the plasma plume with

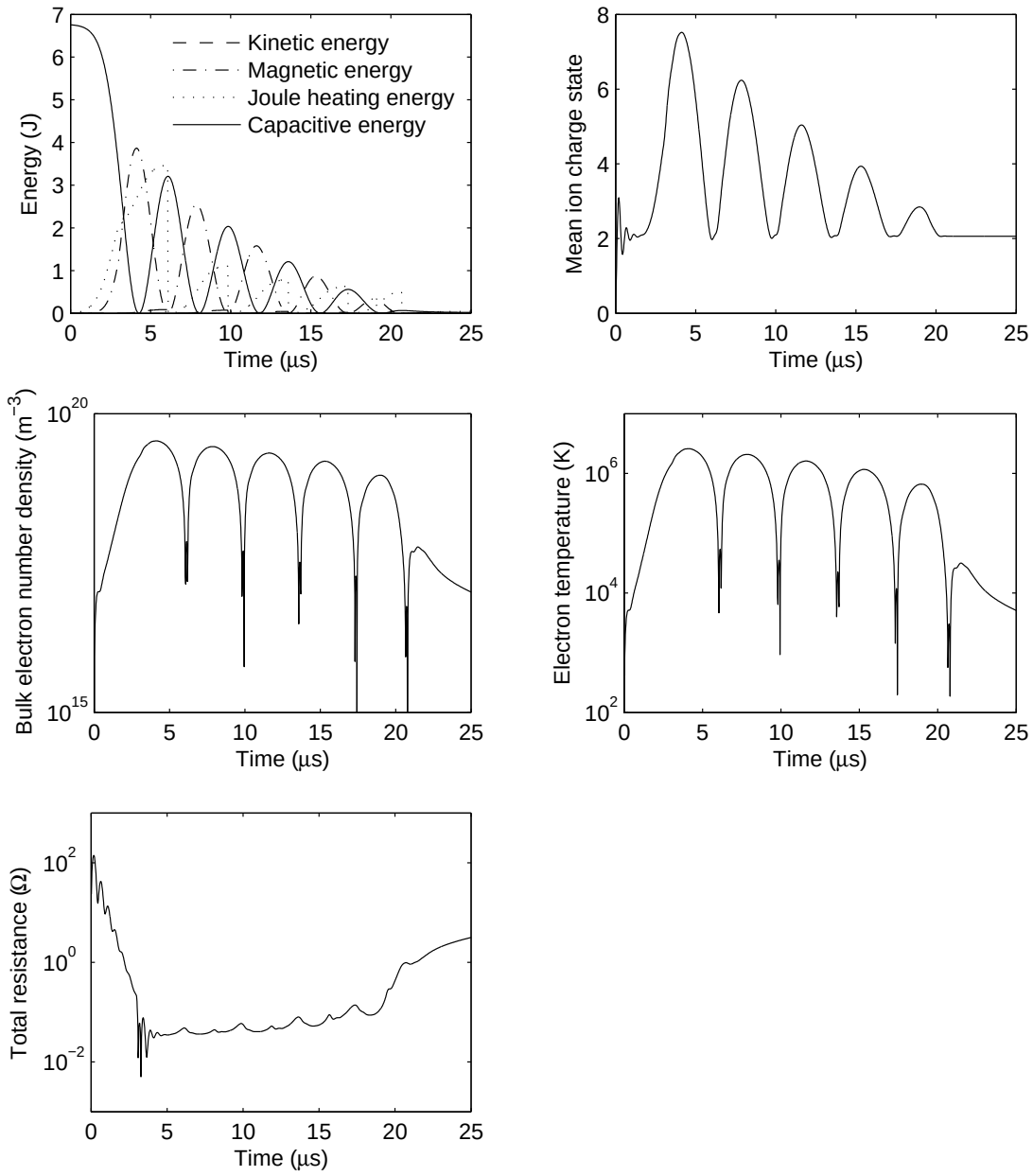

Figure 11: Modeled evolution of the energy processes, the mean ion charge state, the bulk electron number density, the electron temperature and the total circuit resistance during a 6.8J discharge at an electrode spacing of 3cm

a triple Langmuir probe [35]. The individual plasma sheets are indistinguishable in Zwahlens data but the electron number density profile is comparable to that of a 5J discharge where it was recorded that the electron density rapidly increased to a peak in the 10^{-19} to 10^{-20}m^{-3} range and then gradually decreased over the course of the discharge period, similar to the modeled results presented in this work.

Conclusions

An investigation into the phenomena of a PPT discharging without the Teflon propellant suggests that the Plasma mass from most PPTs originate from the erosion of the metal electrodes via the process of cathode spot emission. The model was based on a one dimension circuit analysis model with the inclusion of a variable resistance model, a mass ablation model and realising that the overall plasma discharge is a collection of individual plasma sheets. The model was found to predict current profiles within experimental error when compared to measured data with only a few discrepancies. Modeled plasma parameters are comparable with those found within existing literature. Future work will focus on using the

model to predict PPT characteristics and to use the model as an engineering tool to optimise a future PPT for small satellite operations.

References

[1] Benson, S. W., Arrington, L., Hoskins, W. A., and Meckel, N. J., "Development of a PPT for the EO-1 Spacecraft," *35th Joint propulsion conference*, AIAA-99-2276, Los Angeles, California, 2000.

[2] Rayburn, C. D., Campbell, M. E., Hoskins, W. A., and Cassady, R. J., "Development of a Micro Pulsed Plasma Thruster for the Dawgstar Nanosatellite," *36th Joint propulsion conference*, AIAA-2000-3256, Huntsville, Alabama, 2000.

[3] Nawaz, A., Auweter-Kurtz, M., Kurtz, H. L., and Wagner, H. P., "Pulsed Plasma Thrusters for Primary Propulsion and Attitude Control of a Small All Electrical Satellite," *4th International spacecraft propulsion conference*, ESA SP-555, Cagliari, Sardinia, Italy, 2004.

[4] Tahara, H., "Development of Electrothermal Pulsed Plasma Thrusters for OIT Electric-Rocket-Engine Onboard Small Space Ship," *44th Joint propulsion conference*, AIAA 2008-4643, Hartford, CT, 2008.

[5] Markusic, T., Thio, Y. C. F., and Cassibry, J. T., "Design of a High-Energy, Two-Stage Pulsed Plasma Thruster," *38th Joint propulsion conference*, AIAA-2002-4125, Indianapolis, Indiana, 2002.

[6] Nawaz, A., Herdrich, G., Kurtz, H. L., Schonherr, T., and Auweter-Kurtz, M., "SIMP-LEX: Systematic Geometry Variation Using Thrust Balance Measurements," *30th International electric propulsion conference*, IEPC-2007-168, Florence, Italy, 2007.

[7] Spanjers, G. G., Bromaghim, D. R., Lake, J., Dulligan, M., White, D., Schilling, J. H., Bushman, S., Antonsen, E. L., Burton, R. L., Keidar, M., and Boyd, I. D., "AFRL Micro PPT Development for Small Spacecraft Propulsion," *38th Joint propulsion conference*, AIAA 2002-3974, Indianapolis, Indiana, 2002.

[8] Cooley, J. and Choueiri, E. Y., "Fundamentals of PPT Discharge Initiation: Undervoltage Breakdown through Electron Pulse Injection," *Joint propulsion conference AIAA-2003-5027*, Huntsville, Alabama, 2003.

[9] Gulczinski III, F. S., Dulligan, M., Lake, J., and Spanjers, G. G., "Micropropulsion Research at AFRL," *36th Joint propulsion conference*, AIAA 2000-3255, Huntsville, Alabama, 2000.

[10] Anders, A., *Cathodic Arcs: From Fractal Spots to Energetic Condensation*, Atomic, Optical and Plasma Physics 50, Springer, 1st ed., 2008.

[11] Keidar, M., Boyd, I. D., and Beilis, I. I., "Ionisation and Ablation Phenomena in an Ablative Plasma Accelerator," *Journal of Applied Physics*, Vol. 96, No. 10, 2004, pp. 5420–5428.

[12] Alexeev, Y. A., Kazeev, M. N., and Kozlov, V. F., "Propellant Energy Flux Measurements in Pulsed Plasma Thruster," *International electric propulsion conference*, IEPC 2003-39, 2003.

[13] Nawaz, A., Bauder, U., Bohrk, H. K., Herdrich, G., and Auweter-Kurtz, M., "Electrostatic Probe and Camera Measurements for Modeling the IMPD SIMP-LEX," *Jet propulsion conference*, AIAA 2007-5280, 2007.

[14] Keidar, M., Boyd, I. D., and Beilis, I. I., "On the Model of Teflon Ablation in an Ablation-Controlled Discharge," *Journal of Physics D: Applied Physics*, Vol. 34, 2001, pp. 1675–1677.

[15] Awadallah, R. S., Freund, D. E., and Simon, D., "Electromagnetic Emission Modelling for Micro Pulsed Plasma Thrusters," *41st Joint propulsion conference*, AIAA 2005-3698, Tucson, Arizona, 2005.

[16] Surzhikov, S. T. and Gatsonis, N. A., "A Splitting Method of Unsteady 3-D Magnetogasdynamic Flows Applied to Pulsed Plasma Thruster Plumes," *32nd Plasmadynamics and lasers conference*, AIAA-2001-2743, Anaheim, California, 2001.

[17] Rhodes, R., Keefer, D., and Thomas, H., "A Numerical Study of a Pulsed Plasma Thruster," *37th Joint propulsion conference*, AIAA-2001-3895, Salt Lake City, Utah, 2001.

[18] Rooney, D., Moeller, T., Keefer, D., Rhodes, R., and Merkle, C., "Experimental and Computer Studies of a Pulsed Plasma Accelerator," *43rd Joint propulsion conference*, AIAA 2007-5225, Cincinnati, Ohio, 2007.

[19] Laperriere, D. D., Gatsonis, N. A., and Demetriou, M. A., "Electromechanical Modelling of Applied Field Micro Pulsed Plasma Thrusters," *41st Joint propulsion conference*, AIAA 2005-4077, Tucson, Arizona, 2005.

[20] Ziemer, J. K. and Choueiri, E. Y., "Scaling Laws for Electromagnetic Pulsed Plasma Thrusters," *Plasma Sources Sci. Technol.*, Vol. 10, 2001, pp. 395–405.

[21] Anders, A., Anders, S., Forsters, A., and Brown, I. G., "Pressure Ionisation: Its Role in Metal Vapour Vacuum Arc Plasma and Ion Sources," *Plasma Sources Sci. Technol.*, Vol. 1, 1992, pp. 263–270.

[22] Krinberg, I. A. and Paperny, V., "Cathode Jet Pinching as the Effective Mechanism of Plasma Heating and Acceleration," *IEEE 19th International symposium on discharges and electrical insulation in vacuum*, 2000, pp. 297 – 304 vol.1.

[23] Krinberg, I. A. and Paperny, V., "Pinch Effect in Vacuum Arc Plasma Sources under Moderate Discharge Currents," *Journal of Physics D: Applied Physics*, Vol. 35, 2002, pp. 549–562.

[24] Krasov, V. I., Krinberg, I. A., Paperny, V., Korobkin, Y. V., Romanov, I. V., Rupasov, A. A., and Shikanov, A. S., "Ion Acceleration in a High-Current Cathode Plasma Jet Expanding in Vacuum," *Technical Physics Letters*, Vol. 33, No. 11, 2007, pp. 941–944.

[25] Anders, A., Yushkov, G. Y., Oks, E., Nikolaev, A., and Brown, I. G., "Ion Charge State Distributions of Pulsed Vacuum Arc Plasmas in Strong Magnetic Fields," *Review of Scientific*, Vol. 69, No. 3, 1998, pp. 1332–1335.

[26] Oks, E., Anders, A., Brown, I. G., Dickenson, M., and MacGill, R., "Influence of a Strong Pulsed Magnetic Field on the Charge State Distribution of Ions in a Vacuum Arc Plasma," *17th International symposium on discharges and electrical insulation in vacuum*, 1996, pp. 137–140.

[27] Oks, E., Anders, A., Brown, I. G., Dickenson, M., and MacGill, R., "Ion Charge State Distributions in High Current Vacuum Arc Plasmas in a Magnetic Field," *IEEE Transactions on Plasma Science*, Vol. 24, No. 3, 1996, pp. 1174–1183.

[28] Yushkov, G. Y. and Anders, A., "Extractable, Elevated Ion Charge States in the Transition Regime from Vacuum Sparks to High Current Vacuum Arcs," *Applied Physics Letters*, Vol. 92, No. 041502, 2008.

[29] Wang, L., Jia, S., Shi, Z., and Rong, M., "Numerical Simulation of Vacuum Arc under Different Axial Magnetic Fields," *Journal of Physics D: Applied Physics*, Vol. 38, 2005, pp. 1034–1041.

[30] Child, C. D., "Discharge from Hot CaO," *Physical Review*, Vol. 32, 1911, pp. 492–511.

[31] Forresters, A. T., editor, *Large Ion Beams*, Wiley, New York, 1988.

[32] Anders, A., "A Periodic Table of Ion Charge-State Distributions Observed in the Transition Region between Vacuum Sparks and Vacuum Arcs," *IEEE Transactions on Plasma Science*, Vol. 29, 2001, pp. 393–398.

[33] Spanjers, G. G., Mcfall, K. A., Gulczinski III, F. S., and Spores, R. A., "Investigation of Propellant Inefficiencies in a Pulsed Plasma Thruster," *32nd Joint propulsion conference*, AIAA-96-2723, Lake Buena Vista, Florida, 1996.

[34] Laperriere, D. D., *Electromechanical Modelling and Open-Loop Control of Parallel-Plate Pulsed Plasma Microthrusters with Applied Magnetic Fields*, Msc, Worcester Polytechnic Institute, 2005.

[35] Zwahlen, J. C., *Investigation of a Pulsed Plasma Thruster Plume Using a Quadruple Langmuir Probe Technique*, Ph.D. thesis, Worcester Polytechnic Institute, 2002.